Full-Color Reflective Filters in a Large Area with a Wide-Band Tunable Absorber Deposited by One-Step Magnetron Sputtering

Yu Bu, XiuMing Bu, FuCong Lyu, Guo Liu, Ge Wu, LuLu Pan, LiZi Cheng, Johnny C. Ho, and Jian Lu*

Full-color reflective filters for large area applications with potentially unprecedented color saturation and excellent mechanical properties deposited by one-step magnetron sputtering are proposed. Conventional reflective color filters with multiple layers of dielectric films cannot simultaneously produce a large area and good mechanical properties due to the complex multiple depositions and the difference in the thermal expansion coefficients among the material layers. Herein, full-spectrum colors are generated by novel Mg-based reflective color filters in a large area of 2 cm × 2 cm with a high hardness of 9.12 GPa, where the filters include an absorber layer with controllable optical constants and a reflective layer with an amorphous structure. The saturation and hue of the produced colors can be controlled by tuning the optical constants and the thickness of the absorber layer. Additionally, the hardness of the Mg-based reflective color filters is increased by the reflective metallic glass layers because they are derived from the same material as the absorber layer. This paradigm can pave the way for the efficient fabrication of large area color filtering devices for diverse applications, such as surface decorations, optical components, color display devices, structural color printing, and photovoltaic cells with optimum efficiency.

1. Introduction

Research on reflective color filters, which reflect specific wavelengths in the visible range, has been widely pursued by a large number of researchers in various fields as a crucial component of applications such as optical display devices,[1–3] structural color printing,[4,5] mobile phone backplanes, optical filters,[6] photodetectors,[7] solar cells,[8,9] automotive components, etc.[10] There are three main physical mechanisms to explain the coloration of material surfaces. The first type is known as intrinsic color, which is determined solely by the electronic band structure of materials. Conventional colorant-pigments have a typical intrinsic color, but they easily fade because of chemical inactivation under prolonged illumination.[11,12] The next category is a structured color filter based on surface plasmon resonance effects, which is a periodic subwavelength array of nanocavity structures that absorb visible light over a range of wavelengths.[13–19] The most commonly used design is metal-insulator-metal (MIM) film stacks, where the layer is nanopatterned by complicated lithographic procedures. Compared to the abovementioned colors based on electronic structure or the plasmonic effect, which are impractical to industrialize due to the complexity, durability and limited size,[14,20] a metal-based reflective color filter is indeed a widely applicable approach to achieve various colors by utilizing optical interference effects in planar thin-film structures.[21–23] This approach provides unique features, such as nonfading, color tenability, and high color brightness, rendering it useful in various practical applications.

Due to their advantages and promising applications, many recent studies have focused on the design of metal-based color filters. For example, Kats et al. deposited several colorful thin films on silica substrates with a bilayer structure, one layer being a reflective Au film on the bottom and the other an absorbing Ge thin film on the outermost surface.[23] The appearance of different colors depends on the thickness of the individual film due to the interference effect. However, the colored films obtained contain precious elements (such as Au or Ag), which are costly and unpractical for large-scale applications.[24] Niyomsoan et al. reported colored Titanium

Y. Bu, F. C. Lyu, Dr. G. Liu, Dr. G. Wu, L. L. Pan, L. Z. Cheng, Prof. J. Lu
Department of Mechanical Engineering
City University of Hong Kong
Hong Kong SAR 999077, China
E-mail: jianlu@cityu.edu.hk

Y. Bu, F. C. Lyu, Dr. G. Liu, Dr. G. Wu, L. L. Pan, L. Z. Cheng, Prof. J. Lu
Centre for Advanced Structural Materials
Shenzhen Research Institute
City University of Hong Kong
Shenzhen 518057, China

X. M. Bu
Department of Physics
City University of Hong Kong
Hong Kong SAR 999077, China

Dr. J. C. Ho
Department of Materials Science and Engineering
City University of Hong Kong
Hong Kong SAR 999077, China

The ORCID identification number(s) for the author(s) of this article can be found under https://doi.org/10.1002/adom.201901626.

**ADVANCED
SCIENCE NEWS**
www.advancedsciencenews.com

**ADVANCED
OPTICAL
MATERIALS**
www.advopticalmat.de

nitride and zirconium nitride decorative thin films, but color variations were limited.[25] Moreover, Yang and coworkers proposed a reflective color filter composed of planar Ni/SiO$_2$/Al layers with good angle insensitivity.[26] Although all the above approaches can be used to generate colors, it is extremely difficult to attain the structural colors with both high purity and good mechanical properties. At the same time, because the difference in the thermal expansion coefficients between the film layers is usually large, residual stress may affect its mechanical properties and limit practical applications.[27–29]

Mg-based metallic glass thin films (MGTFs) are good candidates to improve the mechanical properties due to their advantageous combination of a high strength to weight ratio, low density and excellent biocompatibility. For instance, the work of Wu in our research group successfully demonstrated an approach to fabricate Mg-based thin films with a dual-phase nanostructure that exhibits nearly ideal strength.[30] Zberg and co-workers reported that MgZnCa metallic glass alloy demonstrated great potential for biodegradable implants with a great reduction in hydrogen evolution and the same high tissue compatibility.[31] In addition, Wang developed MgZn-based metallic glass with excellent capability in degrading azo dyes under complex environmental conditions.[32] However, regarding optical properties, little work has been done on the color-related optical properties of Mg-based MGTFs.

Here, a set of colored Mg-based reflective color filters consisting of a thin MgZnCa (MZC) film layer serving as a reflector and a thin MgZnCa oxide layer serving as an absorber are demonstrated. Derived from Wu's technology,[30] a Mg60Zn35Ca5 (at%) alloy system was chosen to be the bottom reflective layer because its good metallic glass forming ability contributes good mechanical properties,[30,31,33–36] and it features sufficiently high reflectivity in the visible range. The absorber layer, the MZC oxide thin film, can be directly attained through a one-step reactive magnetron sputtering method after the deposition of the MZC thin film. Importantly, the optical constants of the absorber thin film can be adjusted by tuning the degree of the MZC oxidation. Furthermore, the reflective color filters can be achieved by a synergistic effect in the oxidized degree and the thickness of the MZC oxide layer, which exhibits a high hardness of 9.12 GPa, with remarkable colors covering the visible range. Our study and understanding of the Mg-based reflective color filters will pave the way for the future development of bilayer reflective color filters for high purity color generation with good mechanical properties via one-step deposition.

2. Results and Discussion

The proposed Mg-based reflective color filter on a large area of 2 cm × 2 cm is shown in **Figure 1**a, exhibiting colors covering the visible range. The high-resolution transmission electron microscopy (HRTEM) images demonstrate the configuration of the reflective color filter composed of the MZC oxide/MZC bilayer film, in which the crystal structure is clearly different, as shown in Figure 1b. The bottom 100 nm MZC layer

has a uniform amorphous structure, which is why MZC was chosen to be the bottom metal layer. MZC films are widely studied MGTFs due to their high strength to weight ratio, low density and corrosion resistance; this film does not contain grain boundaries and dislocations.[34] However, the top MZC oxide (MZCO) layer has a completely nanocrystalline structure with a thickness of ≈300 nm. The fast Fourier transform (FFT) graphs of the HRTEM in inset data Figure 1b show an amorphous ring and the diffraction spots corresponding to the MZC metallic layer and MZC oxide structures, respectively, which are consistent with the descriptions above.

To further identify the elements and mechanical properties of the reflective color filters, energy-dispersive X-ray spectroscopy (EDX) and nanoindention were performed, and the results are shown in **Table 1**. Mg, Zn, Ca were detected, and the composition of the MZC oxide layer is close to the target material, indicating that the sputtering process did not cause significant divergence of the elements. However, some deviation in the elemental composition occurs after the oxygen-free MZC sample is oxidized. In addition, we observe that the contents of magnesium and zinc increase with increasing oxygen flow, while the calcium content decreases. We assume that the surface of the sputtering target was oxidized by a large amount of oxygen, reducing the sputtering yield of calcium oxide.[37] In addition, the oxygen contents increase with increasing oxygen flux, but the oxygen also originates from native chemical absorption of oxygen from the air and substrate; thus, we will discuss this process in detail for the MZC oxide thin films.

The mechanical properties of the samples are also summarized in Table 1. The oxygen-free sample has a relatively low hardness of 6.12 GPa, which is still high for a Mg-based alloy, due to the amorphous structure. The average hardness values for the other samples of 3 O, 7 O, and 10 O are 6.44, 9.12, and 9.64 GPa, respectively, which reveals that the hardness increased with the addition and increase of oxygen flux. As is well known, the most common chemical bonds in oxide materials are covalent bonds, which bind the atoms in oxides materials together. Compared to the covalent bonds, the metallic bonds in metals are much weaker in oxides.[38] Thus, the hardness enhancement is strongly correlated with the formation of strong Mg−O and Zn−O covalent bonds compared to the metallic bonds in the MZC alloy. On the other hand, the adhesion strength between the thin films and substrate is also important for the practical applications. Therefore, the adhesion strength of all prepared samples is obtained by microscratch experiments, and the results are also summarized in Table 1. These results show that the adhesion strength for the samples of 0 O, 3 O, 7 O, and 10 O are 1.05, 1.21, 1.19, and 1.32 N, respectively. Each sample of MZC oxide thin films show similar but still relatively lower adhesion strength compared with the oxygen-free sample due to the lower bombardment energy of O^{2+} with respect to Ar$^+$ during sputtering.[37]

To investigate the optical properties of the top absorptive layer, we deposited a set of single layer MZC oxide films on quartz glasses with oxygen flux values from 3 sccm to 30 sccm. The simulated and measured transmittance spectra for four MZC oxide thin films with different oxygen contents (3 O, 5 O, 7 O, and 10 O) are plotted in **Figure 2**. The overall shape
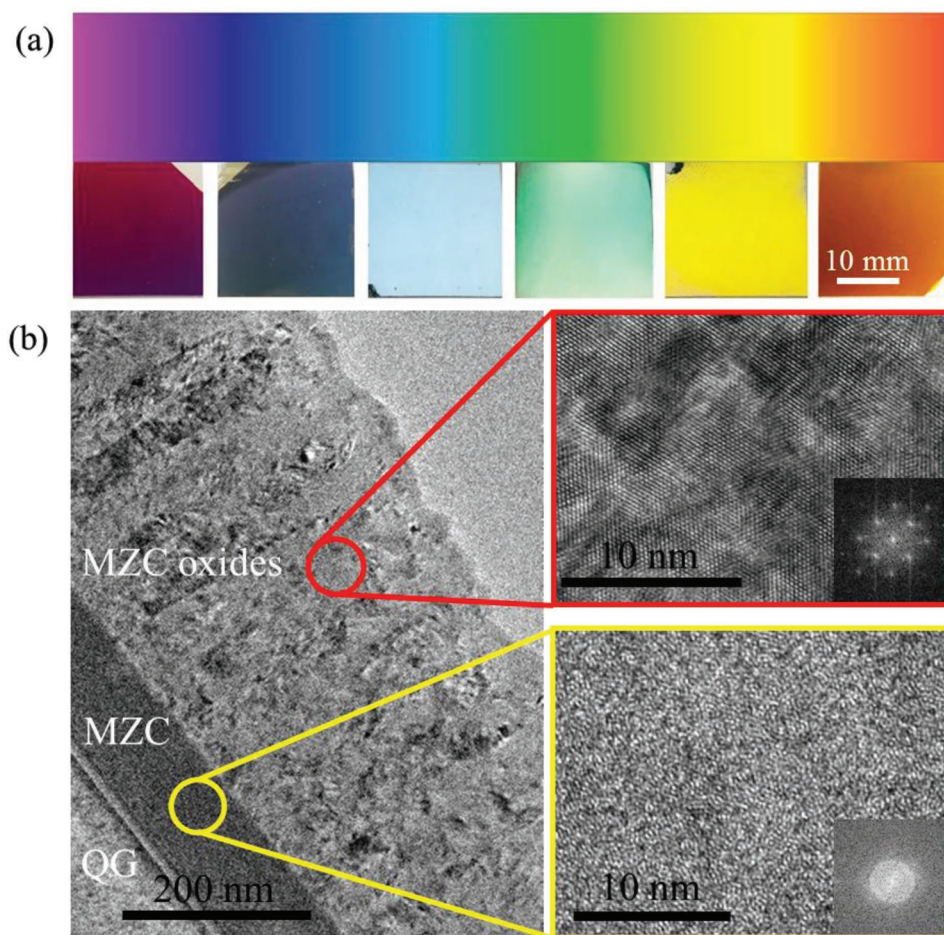
**ADVANCED
SCIENCE NEWS**
www.advancedsciencenews.com

**ADVANCED
OPTICAL
MATERIALS**
www.advopticalmat.de

Figure 1. a) Photos of the MgZnCaO thin films with different colors corresponding to the visible range. b)TEM image of the MgZnCaO thin films.

of each measured spectrum matches quite well with the simulated spectrum with the same oxygen flux. The slight difference between the measured and simulated transmittance spectra can be attributed to the following factors: i) the thickness or refractive-index deviation of the experimental MZC oxide layer, ii) the scattering loss resulting from the uneven surface of the MZC oxide thin film displayed in Figure S1 (Supporting Information), and iii) the measurement inaccuracy resulting from the focusing lens.[39] As shown in Figure 2, when the oxygen flux of deposition remained at a low state (3 O), it exhibited a lower transmittance of 25% compared with the other thin films under higher oxygen flux (5 O, 7 O, and

10 O) due to the insufficient oxidation of the MZC oxide thin film, and the corresponding sample 3 O was dark black. When increasing the oxygen flux to 5 sccm and 7 sccm, the average of the transmittance increased to 40% and 60%, respectively, and the samples changed to semitransparent yellow, as shown in the image. However, the transmittance of the 10 O sample increased to 90%, and the thin film was completely transparent when the oxygen continued to increase to 20 O and 30 O. Based on the above results, this phenomenon is believed to be related to the change in the electronic structure in the MZC oxide layer.[40]

To quantitatively characterize the electronic structure of the MZC oxide layer, the optical energy bandgap (E_g) values of thin films with different oxygen contents were calculated based on the corresponding absorptance spectrum shown in **Figure 3**a. According to bandgap theory, the optical energy gap can be calculated from the absorption coefficient, as expressed [38]

$$A h v = \beta \left(h v - E_g \right)^{1/2} \tag{1}$$

Here, A denotes the absorptance, β denotes a constant, and hv denotes the

Table 1. Composition and adhesion strength of various Mg-based thin films of the same thickness (120 nm) deposited on glass substrates.

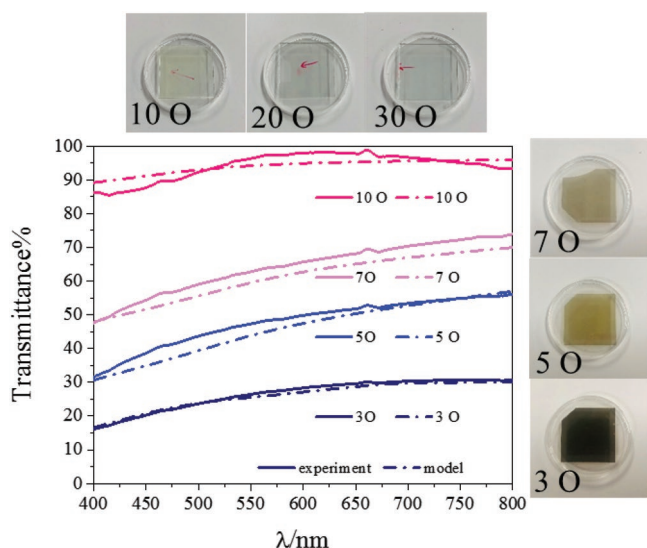| Samples	Concentration [at%]				Hardness [GPa]	Adhesion [N]
	Mg	Zn	Ca	O		
O₂ = 0 sccm	30.42	16.13	3.45		6.12	1.35 ± 0.1
O₂ = 3 sccm	33.37	16.57	2.78	47.18	6.44	1.21 ± 0.1
O₂ = 7 sccm	32.52	15.49	1.29	50.7	9.12	1.19 ± 0.1
O₂ = 10 sccm	30.69	14.64	1.12	53.35	9.64	1.16 ± 0.1

1901626 (3 of 8)

Figure 2. The plot of transmittance of the as-prepared MZCO thin film with lower oxygen flux (3 O, 5 O, and 7 O), photograph of various MZC oxide thin films with different oxygen flow rates.

photon energy, which is calculated from the visible range wavelength.

Therefore, E_g can be deduced from the $h\nu \sim (A\,h\nu)^2$ plots, as illustrated in Figure 3b. Based on the E_g data, a correlation

between E_g and oxygen content is shown. Apparently, E_g increases with decreasing oxygen flux. The 3 O sample, with an E_g (3.92 eV) smaller than the ultraviolet threshold energy (4.2 eV),[1] is therefore semitransparent due to the absorption of part of the visible light. In contrast, the 5 O and 7 O samples exhibit widening bandgaps of ≈4.15 and 4.17 eV, respectively. The samples with higher oxygen flows demonstrate higher bandgaps of ≈4.2 eV or more, corresponding to their high transparency. As a result, a certain threshold energy within the visible region is absorbed, resulting in partial transparency. This result demonstrates that the oxygen reduction changes the electronic structure of the MZC oxide thin film, leading to the colorization of the thin films. Therefore, we assume that the oxygen vacancy concentration in the film may be different.

To further investigate the electronic structure evolution and provide additional evidence of the presence of oxygen vacancies in these oxide thin films, electron spin resonance (ESR) tests were performed, as shown in Figure 3c. The signal observed at ≈299.96 mT can be assigned to the contribution from unpaired electrons, where a higher intensity indicates more vacancies.[41–43] The ESR intensity gradually decreased for samples 3 O, 5 O, and 7 O, indicating that their O vacancies decreased, which is consistent with our absorption results. Thus, from the above results, we confirm that MZC oxides thin films with different oxygen vacancies were successfully fabricated by magnetron sputtering with different ratios of oxygen atmosphere, resulting in the semitransparent oxide thin films.
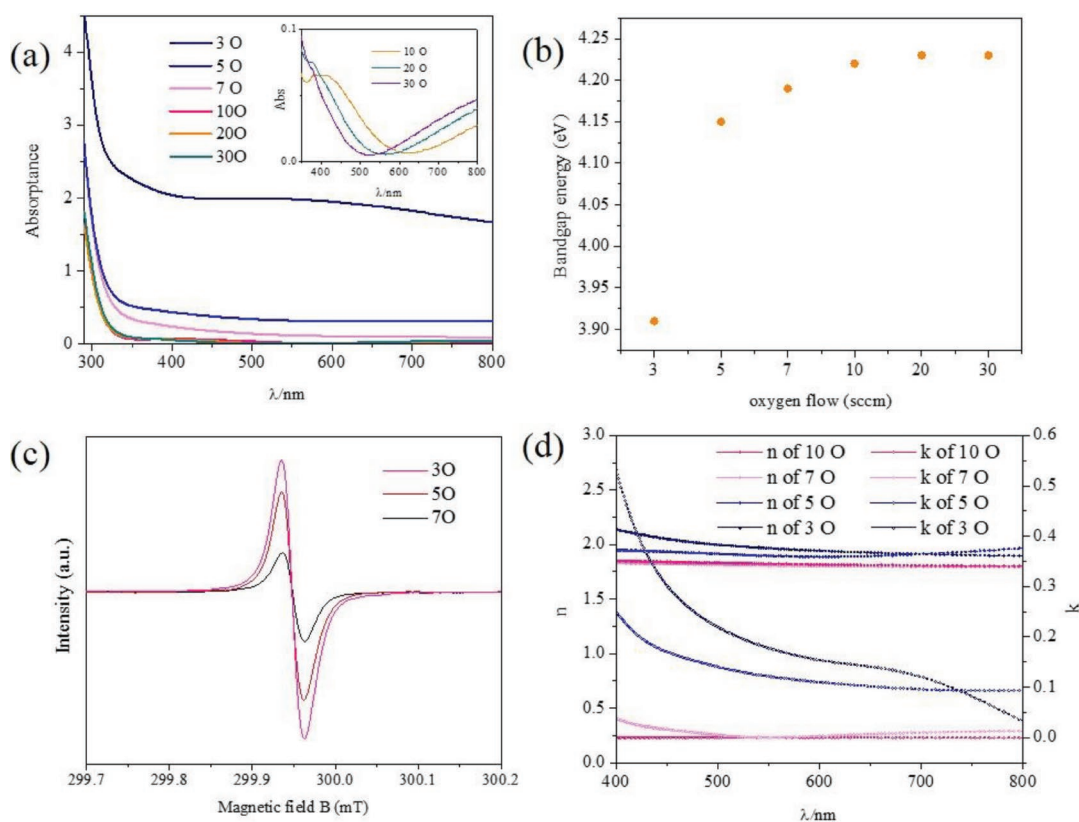

Figure 3. a) The plot of absorptance of the as-prepared MZCO thin film with different oxygen flux values (3 O, 5 O, and 7 O). b) Relationship between the energy band gap and oxygen flow rates of the MZC oxide thin film. c) Uncoordinated electron concentration in different oxygen thin films. d) Optical constants of as-prepared MZC oxide thin film with different oxygen flux values.
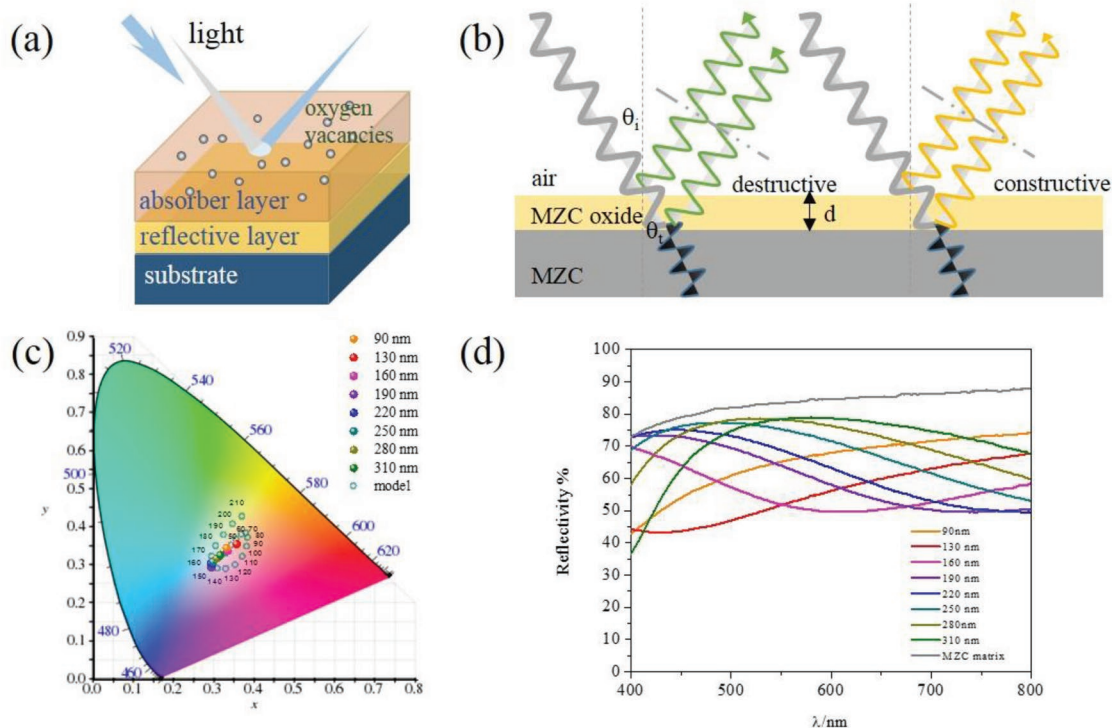
Figure 4. a) Schematic of coloration mechanism in the Mg-based color filter. b) Schematic of the interference effect in Mg-based thin films. c) CIE 1931 chromaticity diagram of samples with different thicknesses. d) Reflectivity spectra of samples with different thickness under the same oxygen flux (10 sccm).

To better understand the optical properties of the MZC oxide thin films, the optical constants were measured by ellipsometry.[23] The refractive index, n, determines the phase change of the light waves reflected from the air/film and film/substrate interfaces, and the extinction coefficient, k, could also provide the energy absorption at the visible frequency of MZC oxides thin films. According to the summarized results in Figure 3d, the average refractive index of the MZC oxides of 3 O, 5 O, 7 O, and 10 O is ≈1.9, which falls into the range between the refractive index of magnesium oxide (1.7) and zinc oxide (2.0). The refractive index of 3 O MZC oxides is the highest at the lower wavelengths, ≈2.13, and reaches a minimum value of ≈1.88 at ≈800 nm. The optical constants of thin films prepared under the low oxygen condition of 5 O are also close to 1.95. The optical constants of the thin films prepared under high oxygen flux conditions of 7 O and 10 O are ≈1.85, lower than the samples with the low oxygen atmosphere. The extinction coefficient of 3 O MZC oxides, which determines the absorption of light, changes between 0.1 and 0.5, indicating that the absorption processes is dominated by the oxygen vacancies in the thin film. The MZC oxides absorb more energy in the blue part of the spectrum and relatively less energy in the yellow to the red part. This observation is in agreement with the phenomenon observed in the absorptance curves. In contrast, the MZC oxide thin film deposited under high oxygen flow (10 O) exhibits a low extinction coefficient close to zero in the visible range, which corresponds to the fully transparent MZC oxide thin films.

The schematic configuration of the proposed Mg-based reflective color filters is shown in **Figure 4**a. The formation of intense interference colors is achieved via depositing an absorber layer (MZC oxide thin film) over a reflective layer (MZC layer). The interference effect occurs when the light is reflected from interfaces in the stack of thin films.[44] In such a case, visible light can be separated into two parts: one part is reflected at the air/MZC oxide thin film interface, and the other part penetrates into the MZC oxide thin film and is ultimately reflected at the MZC oxides thin film/MZC substrate interface, as shown in Figure 4b. The constructive interference between the reflected light from the MZC oxide thin film surface and the emergent light reflected on the MZC oxide thin films-substrate interface causes the different colors. As the colors of the samples are mainly determined by the interference band with the maximum reflectance in the visible region, the wavelength at the maximum reflectance in each interference band can be obtained by[38]

$$\lambda = 2nd/m \tag{2}$$

where m is the interference order, and n and d are the refractive index and thickness of the thin films, respectively. Therefore, it is clear from Equation (2) that λ changes with the film thickness, d, resulting in the alteration of the color of the thin films. According to Equation (2), reflectance depends on the optical constants of the thin film and reflective substrate and on the thickness of the thin film.
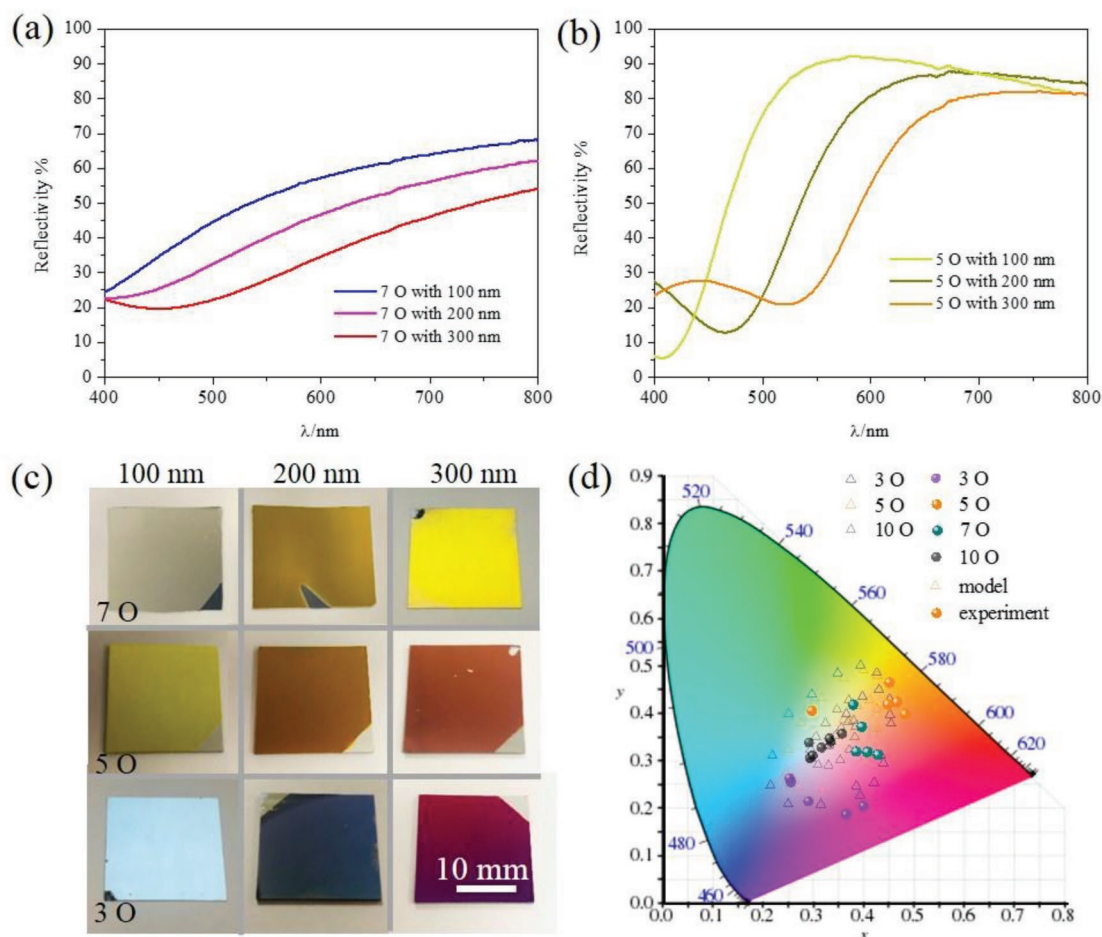
ADVANCED
SCIENCE NEWS
www.advancedsciencenews.com

**ADVANCED
OPTICAL
MATERIALS**
www.advopticalmat.de

Figure 5. a,b) Reflectivity spectra of samples under the same oxygen flux (7 O and 5 O, respectively) with different thicknesses, and corresponding photograph of the fabricated samples at normal incidence with different top layers. c) Photographs of the corresponding samples of (a) and (b), including 3 O samples as well. d) Chromaticity diagram of the colors of the magnesium-based thin films.

By gradually varying the thickness of the MZC oxide layer, the reflectance peaks and colors can be fine-tuned. The colors of the MZC oxides thin films (10 O) with different thicknesses deposited on MZC metallic glass thin film were measured and are displayed in the CIELAB color space using standard daylight illuminant D65 and 2O colorimetric observer,[45] as shown in Figure 4c. When increasing the thickness of the thin films, the color sensitively shifts from the achromatic point (0.33, 0.33) for the 106 nm thickness toward the purple region (0.3, 0.29) of the chromaticity diagram for the 530 nm thickness. The reflectance was strongly influenced by the thickness of the MZC oxide thin film, while general parameters, such as the refractive index and extinction coefficient, remained constant with the sample of 10 O. To gain further insights into the differences in the optical properties of the MZC oxide thin films with different thicknesses, a detailed study of the reflectivity was carried out by conducting spectrophotometry tests, as shown in Figure 4d. In Figure 4d, the constructive interference of the sample with MZCO thicknesses of 90–310 nm happens at the range of the visible wavelength from 400 to 800 nm, and the order, n, of the interference is 2 according to Equation (2). The reflectance maximum value shifts to longer wavelengths with increasing

thickness of the MZC oxide layer, which corresponds to the results exhibited above.

To investigate the interplay between the oxygen vacancies and thickness in Mg-based reflective color filters, the oxygen flux was set to 3 sccm, 5 sccm, 7 sccm, and 10 sccm in the common experimental conditions with different thicknesses. **Figure 5**a and b show the plots of the reflectivity of Mg-based reflective color filters as a function of wavelength and the thickness of the top layer, in which the thicknesses of the MZC oxide layer were fixed at 100, 200, and 300 nm, respectively, and the oxygen atmosphere was set to be 5 sccm and 7 sccm. The corresponding photographs of the fabricated samples at normal incidence with different top layers are shown in Figure 5c. The reflection intensity in the short wavelength band is always low because of the absorption of the ultraviolet light. Since both the reflection peak and dip redshifted from 400 to 500 nm with increasing MZC oxide layer thickness, the samples show a plain light yellow color for samples of 7 O, as shown in Figure 5c. However, when reducing the oxygen flux to 5 sccm, the samples show bright colors with high purity and color modulation. The reflection intensity increased much higher when tuning the oxygen flux from 7 sccm to 5 sccm. Further

**ADVANCED
SCIENCE NEWS**
www.advancedsciencenews.com

**ADVANCED
OPTICAL
MATERIALS**
www.advopticalmat.de

reducing the oxygen flux to 3 sccm, the Mg-based reflective color filters exhibit bright blue to pinkish purple colors, as shown in Figure 5c. Therefore, the oxygen flux of the top MZC oxide layer was chosen to be 5 sccm or 3 sccm to achieve the optimal performance to produce colors with high purity and brightness. The images of the corresponding samples were taken at viewing angles of 0°, 15°, 45°, and 60° and are shown in Figure S2 (Supporting Information). These images further illustrate that Mg-based thin film color filters feature good angle-insensitivity because there is no obvious color change for all samples up to the angle of 60°. To further visualize the color distribution in the samples, the chromatograms of colored magnesium-based thin films are displayed in Figure 5d, which are governed by the synergistic effect of oxygen vacancies and thin film interference. The color of Mg-based thin films deposited under varied oxygen flux values (3 O, 5 O, 7 O, and 10 O) covers the main chromaticity diagram and changes from blue to aqua to deep yellow to burgundy with different thicknesses (50, 100, 150, 200, and 250 nm, respectively) as displayed in CIELAB color space, as shown in Figure 5d. Color spots that exhibit the color variation of the 10 O samples are limited to a small region around the achromatic point, which is consistent with the simulation result of the 10 O thin films with the refractive index of 1.8 and the extinction coefficient of 0.08. However, when reducing the reactive gas flow to 7 sccm, the color spots cover a larger area and reach the yellowish to purple zone with increasing thickness. The thin films color spots reach the border zone when further reducing the oxygen flux to 5 and 3 sccm, corresponding to the trend of the simulation results of the 5 O and 3 O thin films with the refractive index of 1.8 and the extinction coefficients of 0.18 and 0.25, respectively. These results demonstrate that the proposed Mg-based reflective color filters have the potential to achieve all the colors on the chromatogram.

3. Conclusion

Mg-based reflective color filters with a variety of colors covering the visible spectrum and a high hardness of 9.12 GPa were obtained by adjusting the reactive gas flow and the thickness of the thin films through a reactive magnetron sputtering technique. Different color filters over a large area with blue, aqua, gold-like yellow, purple and burgundy were fabricated, consistent with the simulation results. We found that color variation is governed by the synergistic effect of oxygen vacancies and interference between the substrate and the Mg-based thin films. 1) The concentration of oxygen vacancies was dominated via the oxygen flux to obtain controllable optical constants for the MZC oxides thin films; 2) the interference between the reflective layer (MZC) and absorber layer (MZC oxide) in the wavelength-scale-thick film also has an important effect on the coloration. The combination of the interference effect with simple single layer design and the use of the MZC metallic glass thin film serving as the reflector layer and mechanical support offers attractive opportunities for advanced decorative applications. The prepared Mg-based reflective color filters can be used either for adding functionality to protective coatings or for the design of advanced decorative coatings.

4. Experimental Section

Film Preparation: The quartz glass sheets were ultrasonically cleaned with acetone, absolute ethyl alcohol, and deionized water for 30 min. Before the deposition of the MgZnCa oxide thin film, the MZC metallic glass thin film was initially deposited on the quartz glass substrates using DC magnetron sputtering method to reduce the thermal stress caused by heat and served as the reflector layer. The film thickness of MZC was ≈100 nm. The MZC oxide thin films were then deposited with various thicknesses on the substrates with the MZC thin film by RF magnetron sputtering in a mixture of Ar and under different O_2 gas flow rates (purity > 99.99%), with the reactive gas oxygen at 0 sccm (0 O), 3 sccm (3 O), 5 sccm (5 O), 7 sccm (7 O), 10 sccm (10 O), 20 sccm (20 O), and 30 sccm (30 O). During this process, the argon flow rate was 70 sccm, the working pressure was 0.5 Pa, the DC sputtering power for MZC was 120 W, the RF sputtering power for MZC oxides was 80 W, the deposition rate of MZC was ≈9 nm min^{-1}, and the substrate temperature was maintained at room temperature. These deposition conditions were kept constant while the deposition time was varied.

Simulation: For the optical characterization simulation, the TF Calc program was used, and the calculated results were compared with the measured optical properties. The TF Calc simulation procedure is described below. First, construction parameters, such as the refractive index and extinction coefficient of MgZnCa oxides, which were measured and calculated using variable-angle spectroscopic ellipsometry, were input. Second, simulations with variable parameters, such as ranges of wavelength (380–780 nm) and number of layers, were designed. Finally, analysis of the effect of each layer with variable thickness and variable optical constants of the MgZnCa oxide thin films from 50 to 300 nm and extinction coefficients from 0 to 0.3, respectively, was performed to determine optical properties appropriate for optimal simulation with system modification.

Characterization: The microstructures of the thin films were examined by transmission electron microscopy (TEM, JEOL 2100) at 200 kV. TEM samples were prepared with focused ion beam (FIB, FEI) equipment. The compositions of the thin films were examined by EDX to determine precise atom ratios of the composition. Uncoordinated electron concentrations in MgZnCa oxide thin films were studied by electron paramagnetic resonance techniques to confirm the oxygen vacancy concentrations. The morphology of the fabricated thin films was observed by field-emission scanning electron microscopy (SEM, FEI) and atom force microscopy (AFM, Bruker).

The mechanical property of hardness was measured by nanoindentation (Hysitron, USA) using a Berkovich diamond tip, where the hardness values were calculated from data of the thin film with the depth of less than 10% of the film thickness to avoid substrate effects. The adhesion strength of various thin films was evaluated by microscratching using a 100 μm radius diamond probe on a tribometer (Bruker, UMT-3) with a loading scale of 0–100 N and a loading rate 60 N min^{-1} in which the critical load leading to the sudden increase in the coefficient of friction (COF) was regarded as the adhesion strength of the film.

Color Measurements: The reflectivity of the samples was measured at room temperature by a spectrophotometer (SHIMADZU-3700). The color of the coatings was quantitatively evaluated by calculating the chromaticity x and y and luminance factor Y from the spectral data of the films in the visible light range using the CIELAB color space standardized by Commission Internationable del'Eclairage. The chromaticity diagram is based on the values x, y, and z, where $x = X/(X + Y + Z)$, $y = Y/(X + Y + Z)$, and $z = Z/(X + Y + Z)$. Note that $x + y + z = 1$; thus, if two values are known, the third can always be calculated, and the z value is usually omitted. The x and y values together constitute the chromaticity of a sample. The chromaticity measurement was performed at a 2° incident angle with the D65 illuminant in the CIE standard. The complex refractive indices were obtained by variable-angle spectroscopic ellipsometry (J.A. Woollam Inc.). Ellipsometric spectra were analyzed by the CompleteEASE software.

Supporting Information

Supporting Information is available from the Wiley Online Library or from the author.

Conflict of Interest

The authors declare no conflict of interest.

Keywords

absorber materials, interference effect, metallic glass thin films, reflective color filters, structural colors

[1] M. A. Kats, F. Capasso, *Laser Photonics Rev.* **2016**, *10*, 735.
[2] K. Liao, X. Hu, Y. Cheng, Z. Yu, Y. Xue, Y. Chen, Q. Gong, *Adv. Opt. Mater.* **2019**, *7*, 1900350.
[3] S. Lv, B. Shanmugavelu, Y. Wang, Q. Mao, Y. Zhao, Y. Yu, J. Hao, Q. Zhang, J. Qiu, S. Zhou, *Adv. Opt. Mater.* **2018**, *6*, 1800881.
[4] S. Daqiqeh Rezaei, J. Ho, A. Naderi, M. Tavakkoli Yaraki, T. Wang, Z. Dong, S. Ramakrishna, J. K. W. Yang, *Adv. Opt. Mater.* **2019**, *7*, 1900735.
[5] H. Liu, J. Xu, H. Wang, Y. Liu, Q. Ruan, Y. Wu, X. Liu, J. K. W. Yang, *Adv. Mater.* **2019**, *31*, 1807900.
[6] K. T. Lee, S. Y. Han, H. J. Park, *Adv. Opt. Mater.* **2017**, *5*, 1700284.
[7] X. Wang, Z. Cheng, K. Xu, H. K. Tsang, J.-B. Xu, *Nat. Photonics* **2013**, *7*, 888.
[8] S. Y. Lee, K. S. Bang, J. W. Lim, *J. Electron. Mater.* **2014**, *43*, 3204.
[9] Y. Kim, J. Son, S. Shafian, K. Kim, J. K. Hyun, *Adv. Opt. Mater.* **2018**, *6*, 1800051.
[10] L. Martinu, O. Zabeida, J. E. Klemberg-Sapieha, *Handbook of Deposition Technologies for Films and Coatings*, Elsevier Ltd., Norwich, NY, USA **2010**.
[11] A. Furrer, M. Seita, R. Spolenak, *Acta Mater.* **2013**, *61*, 2874.
[12] K. Nassau, *Color Res. Appl.* **1987**, *12*, 4.
[13] H. Lee, T. Y. Jeon, S. Y. Lee, S. Y. Lee, S. H. Kim, *Adv. Funct. Mater.* **2018**, *18*, 1706664.
[14] Z. Li, A. W. Clark, J. M. Cooper, *ACS Nano* **2016**, *10*, 492.
[15] X. Duan, S. Kamin, N. Liu, *Nat. Commun.* **2017**, *8*, 14606.
[16] Y. Gu, L. Zhang, J. K. W. Yang, S. P. Yeo, C.-W. Qiu, *Nanoscale* **2015**, *7*, 6409.
[17] D. Fleischman, K. T. Fountaine, C. R. Bukowsky, G. Tagliabue, L. A. Sweatlock, H. A. Atwater, *ACS Photonics* **2019**, *6*, 332.
[18] L. Shao, X. Zhuo, J. Wang, *Adv. Mater.* **2018**, *30*, e1704338.
[19] Y. Ma, W. Zhao, P. She, S. Liu, L. Shen, X. Li, S. Liu, Q. Zhao, W. Huang, W. Wong, *Small Methods* **2019**, *3*, 1900142.
[20] J. A. Schuller, E. S. Barnard, W. Cai, Y. C. Jun, J. S. White, M. L. Brongersma, *Nat. Mater.* **2010**, *9*, 193.
[21] J. H. Lee, G. E. Jang, Y. H. Jun, *Ceram. Int.* **2012**, *38*, S661.
[22] D. K. Diop, L. Simonot, J. Martínez-García, M. Hébert, Y. Lefkir, G. Abadias, P. Guérin, D. Babonneau, N. Destouches, *Appl. Spectrosc.* **2017**, *71*, 1271.
[23] M. A. Kats, R. Blanchard, P. Genevet, F. Capasso, *Nat. Mater.* **2013**, *12*, 20.
[24] G. T. England, C. Russell, E. Shirman, T. Kay, N. Vogel, J. Aizenberg, *Adv. Mater.* **2017**, *29*, 1606876.
[25] S. Niyomsoan, W. Grant, D. Olson, B. Mishra, *Thin Solid Films* **2002**, *415*, 187.
[26] Z. Yang, Y. Chen, Y. Zhou, Y. Wang, P. Dai, X. Zhu, H. Duan, *Adv. Opt. Mater.* **2017**, *5*, 1700029.
[27] K. Ono, M. Wakabayashi, Y. Tsukakoshi, Y. Abe, *Appl. Surf. Sci.* **2016**, *364*, 69.
[28] J. E. Jedrzejowski, P. Baloukas, B. Klemberg-Sapieha, L. Martinu, *J. Vac. Sci. Technol., A* **2004**, *22*, 725.
[29] G. C. Lain, F. Cemin, C. M. Menezes, C. Aguzzoli, I. J. R. Baumvol, S. S. Tomiello, C. A. Figueroa, *Surf. Eng.* **2016**, *32*, 279.
[30] G. Wu, K.-C. Chan, L. Zhu, L. Sun, J. Lu, *Nature* **2017**, *545*, 80.
[31] B. Zberg, P. J. Uggowitzer, J. F. Löffler, *Nat. Mater.* **2009**, *8*, 887.
[32] J. Q. Wang, Y. H. Liu, M. W. Chen, V. L. L. Dmitri, A. Inoue, J. H. Perepezko, *Sci. Rep.* **2012**, *2*, 418.
[33] K. Schlüter, C. Zamponi, N. Hort, K. U. Kainer, E. Quandt, *Corros. Sci.* **2012**, *63*, 234.
[34] B. Movahedi, *Met. Glasses: Form. Prop.* **2016**.
[35] C. H. Chang, C. M. Lee, J. P. Chu, P. K. Liaw, S. C. J. Jang, *Thin Solid Films* **2016**, *616*, 431.
[36] G. Eddy Jai Poinern, S. Brundavanam, D. Fawcett, *Am. J. Biomed. Eng.* **2013**, *2*, 218.
[37] B. Geçici, Ş. Korkmaz, S. Özen, V. Şenay, S. Pat, *Mod. Phys. Lett. B* **2016**, *30*, 1530012.
[38] C. Yang, C. Zhang, L. Liu, *J. Alloys Compd.* **2017**, *728*, 289.
[39] Z. Yang, Y. Zhou, Y. Chen, Y. Wang, P. Dai, Z. Zhang, H. Duan, *Adv. Opt. Mater.* **2016**, *4*, 1196.
[40] D. Wojcieszak, M. Mazur, D. Kaczmarek, B. Szponar, M. Grobelny, M. Kalisz, A. Pelczarska, I. Szczygiel, A. Poniedzialek, M. Osekowska, *Appl. Surf. Sci.* **2016**, *380*, 159.
[41] D. Gao, G. Yang, J. Zhang, Z. Zhu, M. Si, D. Xue, *Appl. Phys. Lett.* **2011**, *99*, 052502.
[42] B. Panigrahy, M. Aslam, D. S. Misra, M. Ghosh, D. Bahadur, *Adv. Funct. Mater.* **2010**, *20*, 1161.
[43] J. Zhang, W. Xiao, P. Xi, S. Xi, Y. Du, D. Gao, J. Ding, *ACS Energy Lett.* **2017**, *2*, 1022.
[44] S. Kinoshita, S. Yoshioka, *ChemPhysChem* **2005**, *6*, 1443.
[45] J. Gil-Rosta, F. Yubero, R. Fernández, T. Vilajoana, P. Artús, J. C. Dürsteler, J. Cotrino, I. Ortega, A. R. González-Elipe, *Opt. Mater. Express* **2011**, *1*, 1100.